



This is a repository copy of *Modelling and analysis of electrical impedance myography of the lateral tongue*.

White Rose Research Online URL for this paper:
<http://eprints.whiterose.ac.uk/169988/>

Version: Published Version

Article:

Schooling, C.N., Jamie Healey, T., McDonough, H.E. et al. (5 more authors) (2020)
Modelling and analysis of electrical impedance myography of the lateral tongue.
Physiological Measurement, 41 (12). 125008. ISSN 0967-3334

<https://doi.org/10.1088/1361-6579/abcb9b>

Reuse

This article is distributed under the terms of the Creative Commons Attribution (CC BY) licence. This licence allows you to distribute, remix, tweak, and build upon the work, even commercially, as long as you credit the authors for the original work. More information and the full terms of the licence here:
<https://creativecommons.org/licenses/>

Takedown

If you consider content in White Rose Research Online to be in breach of UK law, please notify us by emailing eprints@whiterose.ac.uk including the URL of the record and the reason for the withdrawal request.



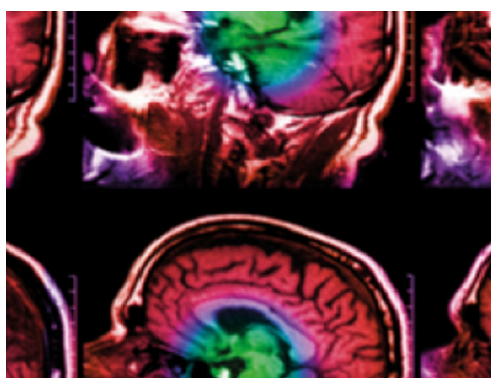
eprints@whiterose.ac.uk
<https://eprints.whiterose.ac.uk/>

PAPER • OPEN ACCESS

Modelling and analysis of electrical impedance myography of the lateral tongue

To cite this article: Chlöe N Schooling *et al* 2020 *Physiol. Meas.* **41** 125008

View the [article online](#) for updates and enhancements.



IPEM | IOP

Series in Physics and Engineering in Medicine and Biology

Your publishing choice in medical physics,
biomedical engineering and related subjects.

Start exploring the collection—download the
first chapter of every title for free.



PAPER

OPEN ACCESS

RECEIVED
23 September 2020REVISED
6 November 2020ACCEPTED FOR PUBLICATION
18 November 2020PUBLISHED
29 December 2020

Original Content from
this work may be used
under the terms of the
[Creative Commons
Attribution 4.0 licence](#).

Any further distribution
of this work must
maintain attribution to
the author(s) and the title
of the work, journal
citation and DOI.



Modelling and analysis of electrical impedance myography of the lateral tongue

Chl e N Schooling^{1,2}, T Jamie Healey³, Harry E McDonough¹, Sophie J French¹, Christopher J McDermott¹, Pamela J Shaw¹, Visakan Kadirkamanathan² and James J P Alix¹

¹ Sheffield Institute for Translational Neuroscience, University of Sheffield, Sheffield, United Kingdom

² Department of Automatic Control and Systems Engineering, University of Sheffield, Sheffield, United Kingdom

³ Department of Clinical Engineering, Sheffield Teaching Hospitals NHS Foundation Trust, Sheffield, United Kingdom

E-mail: cnschooling1@sheffield.ac.uk

Keywords: electrical impedance myography, amyotrophic lateral sclerosis, biomarker, electrodes, finite element modelling, muscle, tongue

Abstract

Objective: Electrical impedance myography (EIM) performed on the centre of the tongue shows promise in detecting amyotrophic lateral sclerosis (ALS). Lateral recordings may improve diagnostic performance and provide pathophysiological insights through the assessment of asymmetry. However, it is not known if electrode proximity to the muscle edge, or electrode rotation, distort spectra. We evaluated this using finite element-based modelling. **Approach:** Nine thousand EIM from patients and healthy volunteers were used to develop a finite element model for phase and magnitude. Simulations varied electrode proximity to the muscle edge and electrode rotation. LT-Spice simulations assessed disease effects. Patient data were assessed for reliability, agreement and classification performance. **Main results:** No effect on phase spectra was seen if all electrodes remained in contact with the tissue. Small effects on magnitude were observed. Cole-Cole circuit simulations indicated capacitance reduced with disease severity. Lateral tongue muscle recordings in both patients and healthy volunteers were reproducible and symmetrical. Combined lateral/central tongue EIM improved disease classification compared to either placement alone. **Significance:** Lateral EIM tongue measurements using phase angle are feasible. Such measurements are reliable, find no evidence of tongue muscle asymmetry in ALS and improve disease classification. Lateral measurements enhance tongue EIM in ALS.

1. Introduction

Amyotrophic lateral sclerosis (ALS) is a fatal neurodegenerative disorder that not only causes weakness of limb and respiratory muscles, but also weakness of the muscles of speech and swallowing, so-called bulbar disease. The use of electrical impedance myography (EIM) as a disease biomarker in amyotrophic lateral sclerosis for both limb and bulbar muscles has been well demonstrated (Alix *et al* 2020, Shellikeri *et al* 2015, McIlduff *et al* 2017, Rutkove 2009, Rutkove *et al* 2007). Development of bulbar muscle biomarkers is particularly important as there are few biomarkers offering an objective measure of bulbar disease (Benatar *et al* 2016). EIM has the capacity to accurately identify and measure disease progression (Alix *et al* 2020, Shefner *et al* 2018); thus, it may be of benefit both in clinical practice and research.

Impedance measurements in the bulbar region in patients with ALS have focused on the tongue. A novel impedance device was used to take recordings in both 2D and 3D electrode configurations as a means to obtain potential 3D structural information. So far, recordings have been reported for measurements made in the midline of the tongue (Alix *et al* 2020, Shellikeri *et al* 2015, McIlduff *et al* 2017, Pacheck *et al* 2016); it is not known if lateral measurements are feasible or provide clinically useful information. While EIM electrodes can be carefully placed on limb muscles, for example, in relation to bony landmarks (Sanchez *et al* 2016), placement on the tongue is more difficult and could be subject to small rotations of the impedance device. Attempts to undertake recordings on either half of the tongue blade may also be undermined by the

proximity of the electrodes to the tongue edge (Scholz and Anderson 2000, Li *et al* 2019, Hua *et al* 1993). However, if possible, lateral recordings may provide additional diagnostic information, for example, by providing a more complete picture of the health of the muscle. Such recordings would also provide insight into disease pathophysiology, as although limb involvement in ALS is often asymmetrical (Devine *et al* 2014), little is known about the presence/absence of bulbar disease asymmetry.

In this paper we demonstrate that lateral placement and electrode rotation have no significant effect on the impedance phase spectra. To establish this we develop a finite element model of the tongue that achieves a simultaneous fit across multiple electrode configurations. The model is applied to patients with ALS exhibiting different severities of disease and to healthy volunteers. As a result the paper also develops a method for identifying disease and its progression. Using real patient data we show that lateral measurements outperform central measurements in the identification of disease, and that their combination further enhances disease detection.

Herein we describe our impedance data collection process, development of the FEM model and subsequent conclusions. An analysis of the robustness of data obtained through lateral placement is presented, followed by an assessment of disease identification using lateral and central placement data.

2. Methods

2.1. Data collection in human participants

Impedance spectra were recorded from 41 patients with ALS and 30 healthy volunteers (demographics in table 1). Informed consent was obtained and the study was approved by an NHS research ethics committee (reference 15/YH/0121). Data was collected in patients at 3 monthly intervals for up to a year where possible, while healthy volunteers had just one follow up visit 6 months from baseline.

Measurements were taken using a bespoke, handheld bioimpedance tongue device designed and constructed by the Department of Clinical Engineering at Sheffield Teaching Hospitals NHS Foundation Trust (Alix *et al* 2020) (figure 1(a)). Upper and lower electrode plates contained four, 1.5 mm diameter circular, gold electrodes arranged in a square with a 5 mm centre inter-electrode distance and 7 mm plate separation distance. A sinusoidal current (5 μ A root mean square) was injected across 14 frequencies.

Let the dataset for each measurement be $\mathcal{D} = \{Z(f_i) | i = 1, \dots, N_f\}$, where $Z(f_i) = R(f_i) + jX(f_i)$ is the impedance measurements in complex form with $R(f)$ being the resistance and $X(f)$ being the reactance. N_f is the number of frequencies (14) and $f_i = f_1 2^{i-1}$ with $f_1 = 76$ Hz. The impedance magnitude, $|Z(f_i)|$ and impedance phase, $\theta(f_i)$ are subsequently calculated as

$$\theta(f_i) = \arctan \frac{X(f_i)}{R(f_i)}, \quad |Z(f_i)| = \sqrt{R(f_i)^2 + X(f_i)^2}. \quad (1)$$

Multiple studies have demonstrated the impedance phase to be a clinically significant metric (Alix *et al* 2020, Shellikeri *et al* 2015, McIluff *et al* 2017, Rutkove 2009, Rutkove *et al* 2007). However, the potential utility of impedance magnitude should not be discounted; indeed, this metric has been used in other applications of impedance spectroscopy (Anumba *et al* 2020, Khan *et al* 2016). Figure 3 shows clear discrepancies between patients and healthy volunteers in both phase and magnitude spectral patterns. Impedance readings were taken for a number of different measurement configurations. This included measurements in the centre of the tongue as well as with lateral placement both on the left and right sides; measurements repeated with the tongue relaxed inside the mouth (intraoral) and tongue protruded (extraoral); and measurements for all eight electrode configurations (as in figure 1(b)).

For each visit, recordings were made in turn for left, right, then central placement; first in the extraoral configuration followed by the intraoral configuration. To take a second set of measurements (trial 2) this whole process was repeated, thus the probe was removed and replaced several times during a recording session. The six measurement paradigms and eight electrode configurations used means that 48 spectra were generated for each participant visit, therefore the full multi-visit dataset contains over 9000 spectra.

Measurement errors can be caused by poor tongue to electrode contact (see section 3.2.1). During measurements constant observation of electrode contact was made. If electrodes became visible during measurement, then the recording was aborted. Any recordings comprising negative resistance at any frequency were removed; because the tongue is a passive system this would imply that it will behave as a positive real system and, as such, is a good indication that the measurements are artefactual. Next, remaining outlier spectra were removed using a root-mean-squared deviation-based outlier detection algorithm (see appendix A).

Table 1. Demographics of the participant cohort. Note that this paper uses the same impedance dataset as Alix *et al* (2020), which includes further details of clinical and electrophysiological characteristics of the patients. Reprinted from Alix *et al* (2020), Copyright (2020), with permission from © 2020 International Federation of Clinical Neurophysiology. Published by Elsevier B.V. All rights reserved.

Measurement	Patients	Healthy volunteers	<i>P</i> value
	<i>N</i> = 41	<i>N</i> = 30	(statistical test)
Mean age in years	62	56	<i>P</i> = 0.12
(range)	(30–83)	(22–86)	(<i>t</i> -test)
Male:female (<i>n</i>)	22:19	14:16	<i>P</i> = 0.63
(%)	(54:46)	(47:53)	(Fishers test)
Limb onset disease	24 (59%)		
Bulbar onset disease	17 (41%)		

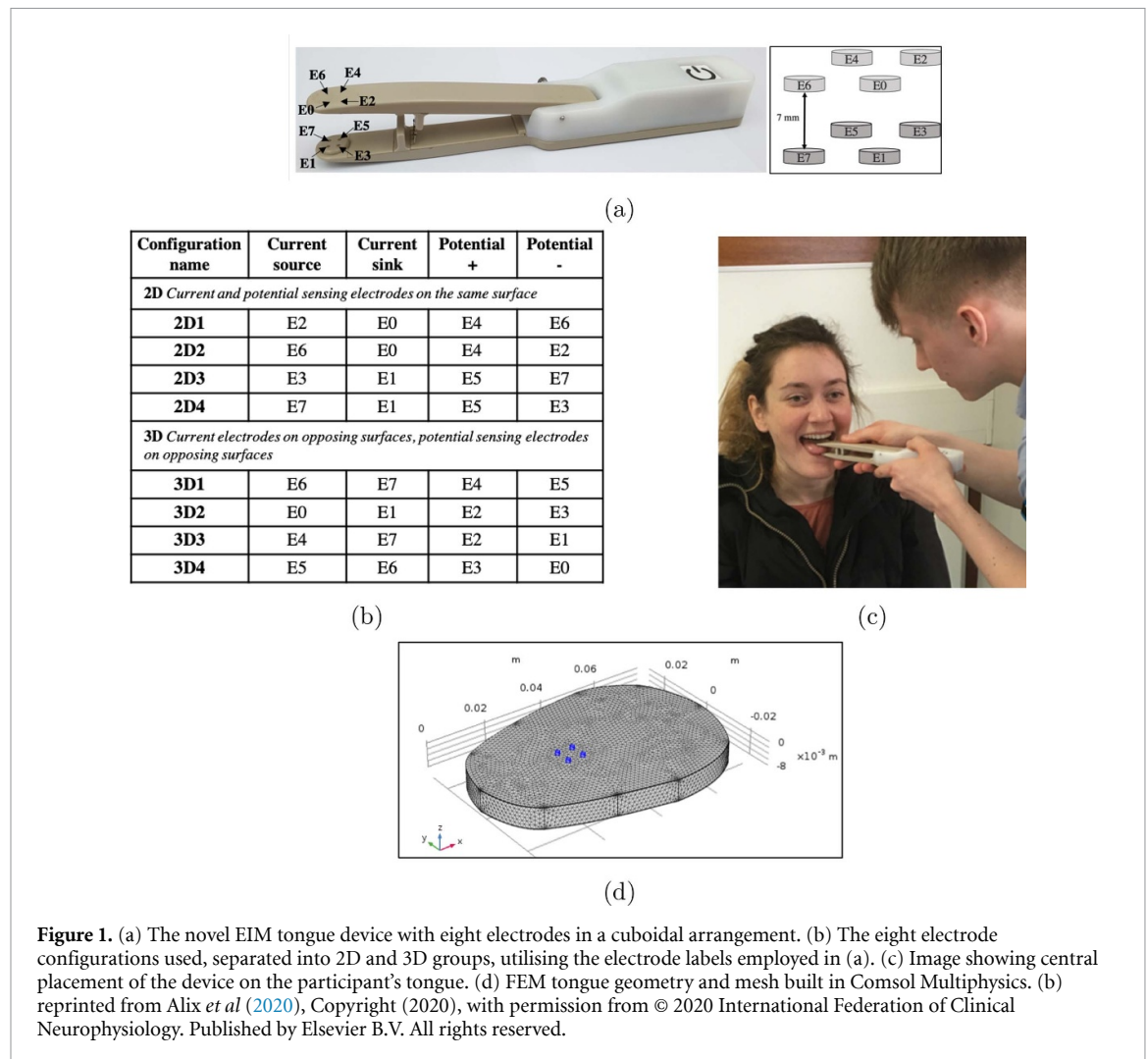


Figure 1. (a) The novel EIM tongue device with eight electrodes in a cuboidal arrangement. (b) The eight electrode configurations used, separated into 2D and 3D groups, utilising the electrode labels employed in (a). (c) Image showing central placement of the device on the participant's tongue. (d) FEM tongue geometry and mesh built in Comsol Multiphysics. (b) reprinted from Alix *et al* (2020), Copyright (2020), with permission from © 2020 International Federation of Clinical Neurophysiology. Published by Elsevier B.V. All rights reserved.

2.2. Grouping patients by symptoms

In order to develop finite element models for different severities of disease, patients were sorted into four symptom groups (figure 2) by combining the ALS functional rating bulbar subscore (ALSFBS), tongue strength, and clinical examination findings (clinical signs of tongue wasting, weakness and fasciculations).

The no symptom group was determined by a maximum (12/12) score on the ALS functional rating scale bulbar subscore and the absence of any abnormal clinical signs. The other groups were obtained through the combination of ALSFBS bulbar subscore, tongue strength and clinical examination. Clinical examination was undertaken by an experienced physician, with scoring described in table 1. Evaluation of tongue strength was undertaken with quantitative muscle testing (QMT) system (Averil Medical), coupled to the Iowa Oral Performance Instrument (IOPI) (Shellikeri *et al* 2015, Easterling *et al* 2013). Briefly, patients were asked to press the small bulb up onto the roof of the mouth as hard as possible for 10 s.

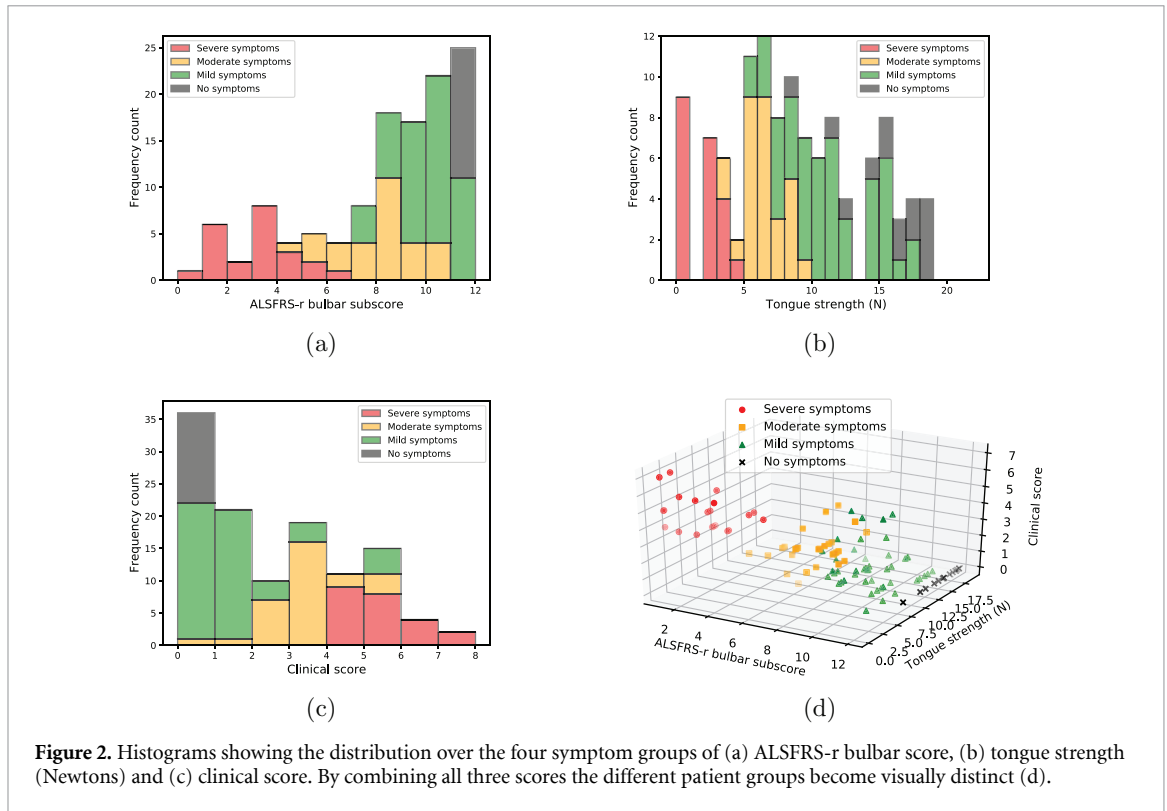


Figure 2. Histograms showing the distribution over the four symptom groups of (a) ALSFRS-r bulbar score, (b) tongue strength (Newtons) and (c) clinical score. By combining all three scores the different patient groups become visually distinct (d).

Assessment of the central placement tongue impedance data was made to evaluate the differences in spectral patterns between these four groups (figure 2). Due to the similarity between healthy volunteers and patients in the no symptom and mild groups, finite element modelling was only applied to healthy volunteers and the moderate and severe patient groups.

2.3. Building the FEM-based model

Finite element method (FEM) based modelling was employed to explore the underlying differences in the electrical properties of the tissue between the different disease states. Model parameters were then attributed to a lumped circuit LT-Spice model to gain further insight into the disease process.

Capturing the detailed structure of the tongue is difficult due to a highly complicated muscle fibre arrangement, with fibres running in multiple directions (Gilbert and Napadow 2005, Gaije *et al* 2007). Here, a simplified tongue geometry was built from layers of tissue with varying electrical conductivity and anisotropy. The shape of the tissue mimics that of a tongue MRI taken from Ong and Chong (2006), with a length of 78 mm and maximum breadth of 56.5 mm, which are reported for the average dimensions of an adult tongue (Hopkin 1967). The muscle is surrounded by a 2 mm epithelium layer (Prestin *et al* 2012), with set value of conductivity spectra (10) taken from reported results for the dorsal and ventral layers (Lackovic and Stare 2007, Richter *et al* 2015). The geometry used is shown in figure 1(d).

The model was developed using the AC/DC module in Comsol Multiphysics software. Modelled local impedance measurements are produced using eight electrodes of 1.5 mm diameter in a cuboidal arrangement analogous to the novel tongue device. The conductivity of the electrodes is set to be much greater than that of the tissue. The finite element mesh was generated automatically with the Comsol software and consisted of 97 155 elements. The model is run to generate spectra for each of the eight electrode configurations in turn, by passing current and reading voltage between different electrode pairs, as laid out in figure 1(b). The 2D configurations pass current and read voltage on the same surface, while the 3D electrodes pass current and read voltage between the upper and lower tongue surfaces.

A frequency domain study was employed with the scalar electric potential as the dependent variable. Magnetic induction effects are assumed to be negligible since they are expected to be approximately six orders of magnitude smaller. The current flow in EIM is the combination of direct current and displacement current ($\vec{J}_{tot} = \vec{J}_c + \vec{J}_d$). Direct current flows due to moving charge particles and is defined as

$$\vec{J}_c(x, y, z) = \sigma(z) \cdot \vec{E}(x, y, z), \quad (2)$$

where x , y and z are the longitudinal, transverse and vertical coordinates of the local current; $\sigma(z)$ is the local conductivity of the tissue, which is assumed to be uniform over x and y but varies with z (different values between the layers of tissue); and $\bar{E}(x, y, z)$ is the local electric field.

An alternating current with amplitude, I_0 and frequency, ω (rad s⁻¹) is passed between a terminal electrode and ground electrode (where the electric potential is set to 0). The displacement current then arises from the changing field induced by this alternating current and is given by

$$\bar{J}_d(x, y, z) = \epsilon \frac{\partial \bar{E}(x, y, z)}{\partial t} = \epsilon_0 \epsilon_r \frac{\partial \bar{E}(x, y, z)}{\partial t}, \quad (3)$$

where ϵ is the permittivity ($\epsilon = \epsilon_0 \epsilon_r$), ϵ_0 is permittivity of free space (8.854×10^{-12}) and ϵ_r is relative permittivity. The phasor representation of the electric field produced by an alternating current is given by

$$\bar{E} = \bar{E}_0 e^{j\omega t} \quad (4)$$

and hence (3) becomes

$$\bar{J}_d = j\omega \epsilon_0 \epsilon_r \bar{E}. \quad (5)$$

For alternating current sources inside conductive media the equation of continuity is then solved:

$$Q = \nabla \cdot \bar{J}_{tot}, \quad (6)$$

where Q is the total charge inside each element. To get a full description of an electromagnetics problem, boundary conditions must be specified at material interfaces. The boundary condition implemented in Comsol, for interfaces between different media with electric field \bar{E}_1 and \bar{E}_2 and outward normal from medium two, \bar{n}_2 is given by

$$\bar{n}_2 \cdot (\bar{E}_1 - \bar{E}_2) = Q. \quad (7)$$

The electric field is related to the potential difference (V) through

$$\bar{E} = -\nabla V, \quad (8)$$

and hence the electrical potential at the electrode surfaces can be output by the FEM.

The local impedance (Z) between a set of electrode pairs at the frequency of excitation current signal is then calculated as

$$Z = \frac{V_1 - V_2}{I_0} \quad (9)$$

where V_1 and V_2 are the potentials at the two electrodes, respectively, as obtained from the FEM model.

2.3.1. Model parameterisation

To provide a parametrisation with potential for interpretation of the parameters, the conductivity spectra for the tissue making up the main body of the tongue is set as the following simplified Cole-Cole equation:

$$\sigma(z \in \Phi_l) = \frac{1}{Z_1^{(l)} + \frac{Z_0^{(l)} - Z_1^{(l)}}{1 + j \frac{f}{F_c^{(l)}}}} \quad (10)$$

where j is the imaginary unit, f ($= \omega/2\pi$) is the frequency (Hz) and $Z_0^{(l)}$, $Z_1^{(l)}$ and $F_c^{(l)}$ are real valued free parameters, which depend on the specific layer of depth, Φ_l . The tongue muscle has anisotropic properties (Gaije *et al* 2007), so different sets of parameters are inputted for the longitudinal, transverse and vertical directions of the tongue.

Since it is possible that fibres run in predominantly different directions at different depths (Benatar *et al* 2016), the tongue body was split into three layers in order to allow enough geometrical complexity for the model fit to data to be achievable. A total of 27 free parameters for conductivity properties were used, with an additional parameter representing the thickness of the middle layer.

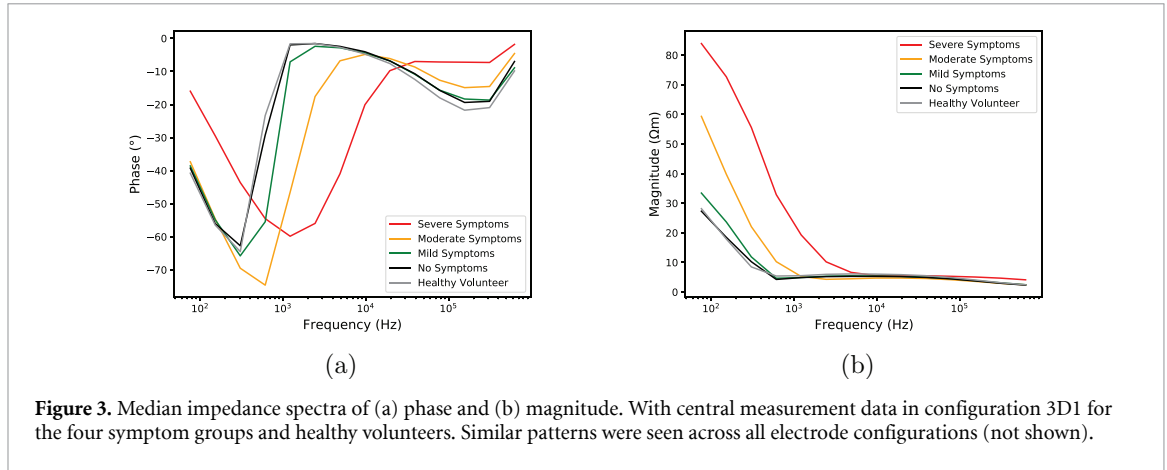


Figure 3. Median impedance spectra of (a) phase and (b) magnitude. With central measurement data in configuration 3D1 for the four symptom groups and healthy volunteers. Similar patterns were seen across all electrode configurations (not shown).

To assess the agreement between the modelled and measured data the normalised root mean squared error (NRMSE) is employed. The NRMSE metric between the impedance measurement (θ , $|Z|$) and model estimate ($\hat{\theta}$, $|\hat{Z}|$) is calculated independently for phase and magnitude as

$$\text{NRMSE} = \frac{\sqrt{\frac{\sum_{i=1}^{N_f} (\alpha_i - \hat{\alpha}_i)^2}{k}}}{\alpha_{\max} - \alpha_{\min}}, \quad (11)$$

where α represents θ or $|Z|$, N_f is the number of measurements in the set (14 frequencies per electrode configuration). Note that calculation on impedance phase is not affected by phase flips since values are automatically constrained between -90° and 90° .

2.4. Disease classification and symptom correlation

Classification analysis between patients and healthy volunteers was undertaken with 3-nearest neighbour and 4-fold cross validation (Bishop 2006). Classification performance was assessed through sensitivity, specificity and the area under the receiver operating characteristics curve (AUROC). Each electrode configuration dataset holds 14 phase values from all frequencies, and two electrode configurations (3D1 and 3D2) data were combined (see section 3.2.2).

Feature selection was made through a wrapper algorithm forward selection approach. This involved building up features one by one using the AUROC as the evaluation criterion. The algorithm then selects the combination of features that gives the optimal results. A maximum of eight selected features was implemented to reduce overfitting.

For comparison of two AUROC values A_1 and A_2 , the Z-score was calculated as

$$\Xi = \frac{(A_1 - A_2)}{\sqrt{SE_1^2 + SE_2^2 - 2Covar[A_1, A_2]}}, \quad (12)$$

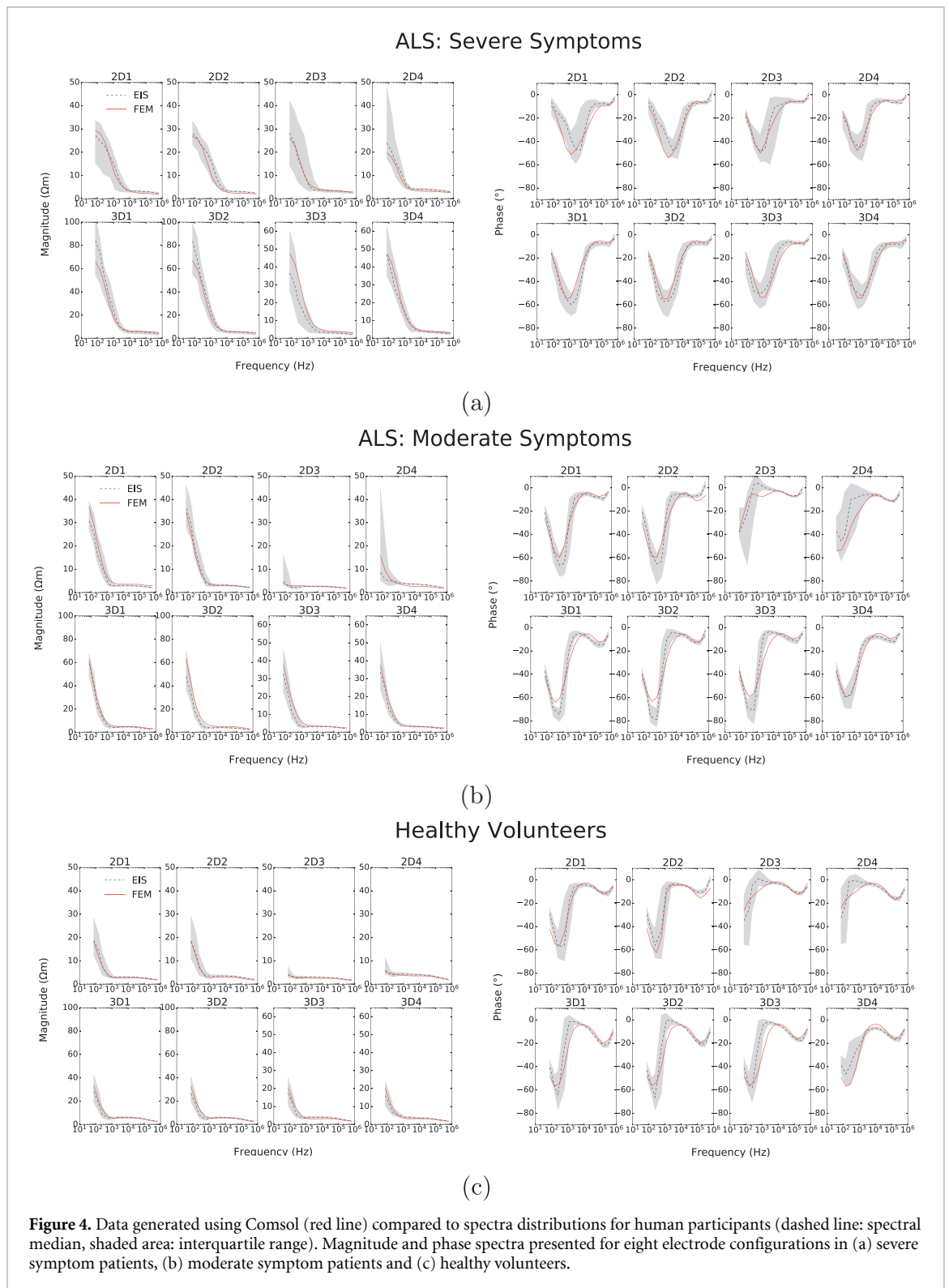
where SE_1 and SE_2 are the standard errors of each AUROC value, and $Covar[A_1, A_2]$ is the covariance of the two AUROCs. These were calculated using methods described in Hanley and Hajian-Tilaki (1997).

In order to assess the correlation of the impedance data with tongue strength, the spectra were reduced into one metric using the L2 (Euclidean) norm. Where again, features were selected through a forward selection wrapper algorithm. The L2 norm is calculated as the square root of the sum of the squared values over the chosen features. The correlation performance was quantified using the Spearman rank correlation coefficient (ρ) which measures the strength and direction of monotonic association between the L2 norm and tongue strength.

3. Results

3.1. Model fit

The parameter values were iteratively adapted so that the model impedance spectra for both phase angle and magnitude were in good agreement with collected data. The patients were split into different disease categories due to differences in the appearance of spectra (figure 3). The parameter optimization was initialised with a trial and error process for a good fit. Following this an iterative local parameter search was made to determine the minimum deviation between the model and collected data. Separate models were



generated for healthy volunteers, patients with moderate disease and patients with severe disease. Producing a simultaneous fit across all electrode configurations for both phase and magnitude was challenging due to the high number of parameters and variables involved. Despite this challenge, a high level of agreement between the observed data and FEM was achieved across all groups for both phase and magnitude (figure 4).

Visual assessment of the residual distributions of the FEM fit demonstrated a random distribution centred around 0 (appendix C1). Calculation of the NRMSE also showed a good fit, with the variation in the phase being around half of the average variation between two repeat measurements (see section 3.2.2 and figure 8). Therefore, the model was deemed to have sufficiently captured the overall electrical properties in different stages of disease.

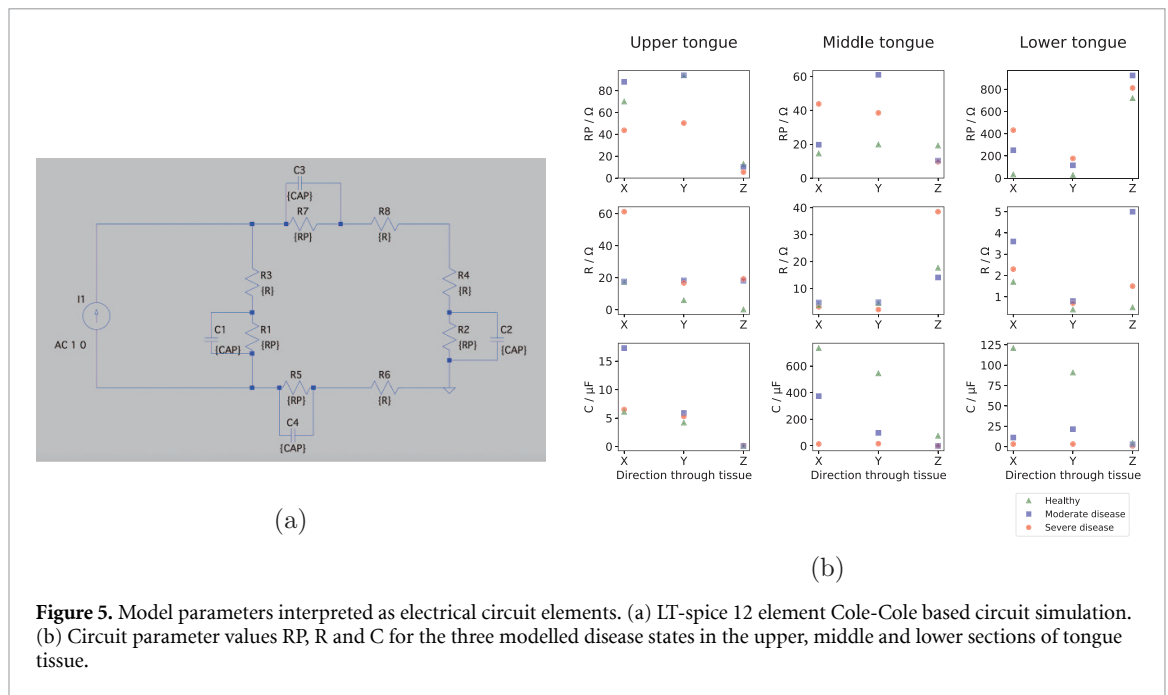


Figure 5. Model parameters interpreted as electrical circuit elements. (a) LT-spice 12 element Cole-Cole based circuit simulation. (b) Circuit parameter values RP, R and C for the three modelled disease states in the upper, middle and lower sections of tongue tissue.

To gain further insight into the effect of the disease process from the external electrical measurements made, we explored reducing the system to a lumped circuit model, similar to that presented in Shiffman and Rutkove (2013a), Shiffman and Rutkove (2013b). The optimised model parameters describing the conductivity spectra of the tongue were fit to a lumped model of a balanced Pi network of four simplified Cole-Cole networks (figure 5(a)). This network was simulated with the LT-Spice simulator using AC small-signal analysis. A NRMSE analysis was undertaken to assess the level of agreement between the FE and LT-spice models. Each set of parameters (Z_0, Z_1, F_C) is then interpreted as an intracellular resistance (RP), extracellular resistance (R) and capacitance (C).

Inspection of the model parameters for the three scenarios (appendix B2) characterises the underlying disease changes to tongue properties and tissue anisotropy. Using LT-Spice simulations these can then be interpreted as circuit parameters varying across the different stages of disease (figure 5). The good agreement (NRMSE < 0.005) between Comsol and Spice demonstrate that the FEM tongue characteristics can accurately be reduced to a lumped model. The most explicit change seen was decreasing capacitance (and hence more negative reactance) with disease progression, mainly due to changes in the x/y directions in the middle and lower tongue sections. The overall effect on extracellular resistance was an increase with disease severity. The intracellular resistance also consistently increased in the lower tongue and the x/y directions of the middle tongue, while the direction of change seen in the upper tongue is less consistent. Overall, these results are in keeping with the known pathophysiology of muscle in ALS (see section 4).

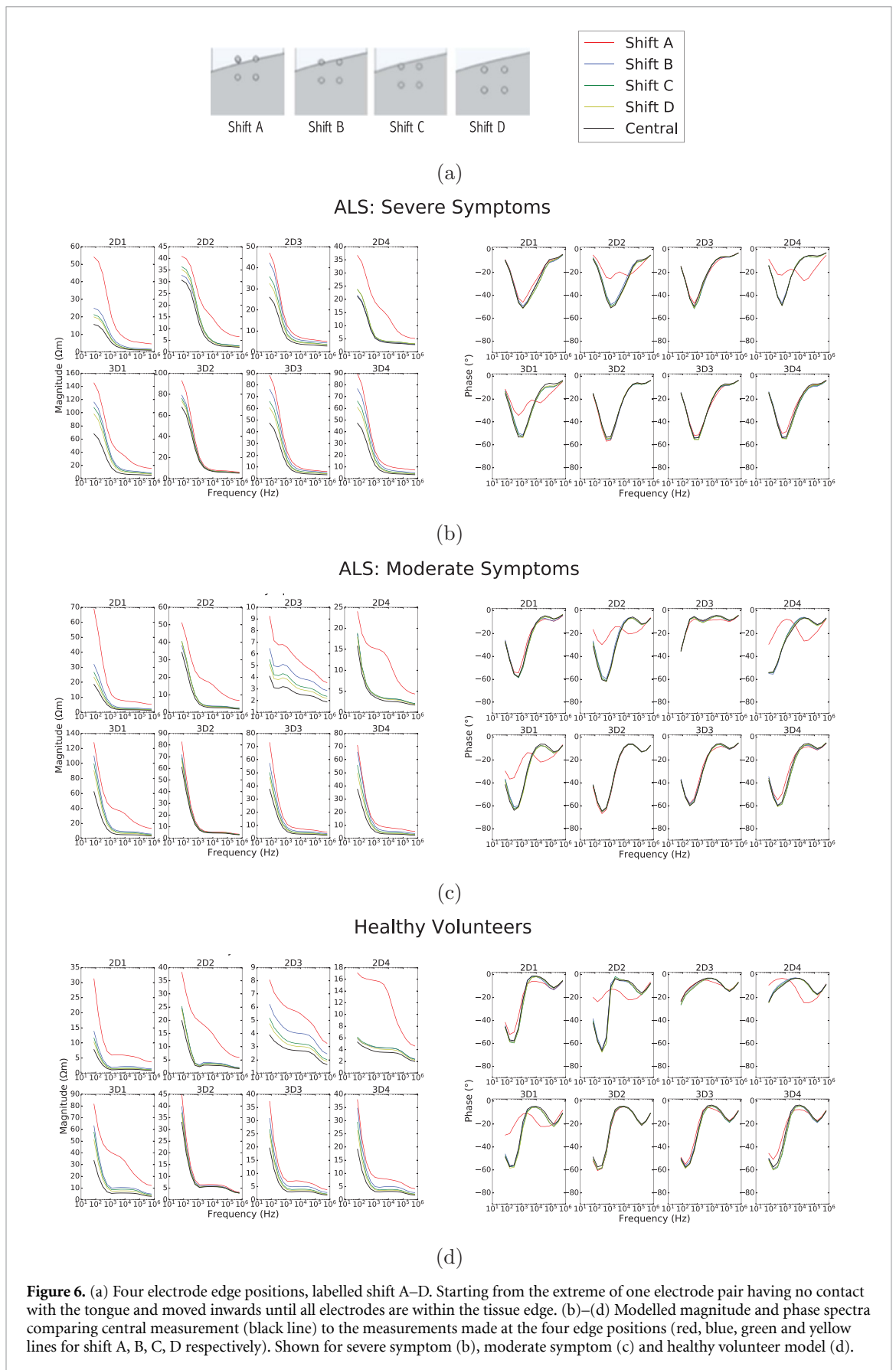
3.2. Robustness analysis of patient measurements

The feasibility of lateral tongue EIM phase angle measurements was interrogated using the FEM. The robustness of patient data was then evaluated through the assessment of similarity/agreement of different measurement configurations, as well as overall measurement reliability.

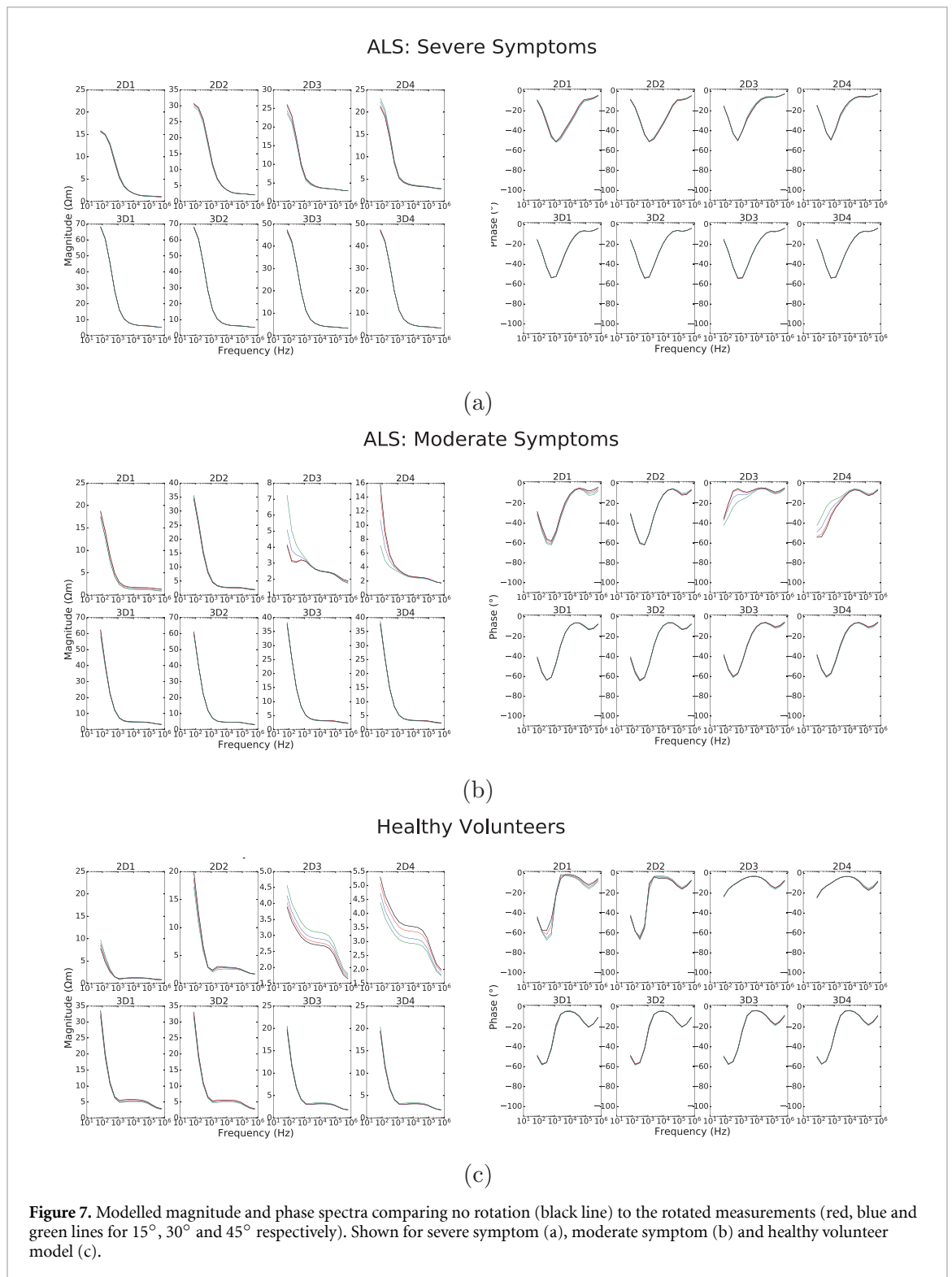
3.2.1. FEM assessment of edge and rotation effects

Using the optimised FEM-based models the effects of moving the electrodes closer to the edge of the tissue were investigated for both impedance magnitude and phase angle. Simulations were run for four edge positions (shift A–D shown in figure 6(a)), starting with the extreme of one electrode pair having no contact with the tongue and moving until all electrodes are in full contact. The data show that the effect on magnitude is greater than that on phase, with the latter only showing obvious changes when electrode contact has been lost (see figure 6, RMSD values presented in appendix B3).

When the electrodes are placed close to the edge of the tongue the path of the currents changes because the current flow is constrained to be within the tongue and not the surrounding air. The results in figure 4 demonstrate that the displacement of the current path changes its magnitude distribution but not its phase, hence for the transferred impedance measurement there is a greater sensitivity to magnitude over phase. It must be noted that all electrodes in use require at least partial contact with the tissue surface. Lack of contact



can result in an extreme change to the phase spectra and, in addition, the instrumentation will not produce reliable results with an open circuit electrode. It is likely that these measurements will likely be excluded in the outlier removal stage (2.5% of lateral measurements were removed as outliers, compared to 1.2% of central measurements).



Since the tongue muscle demonstrates anisotropy between the longitudinal and transverse directions, rotation of the electrode plates during device placement may impact upon the measured impedance spectra. To explore this, the FEM simulated electrode plate rotations by 15°, 30° and 45° (figure 7, RMSD values presented in appendix B4).

Minimal changes to either impedance magnitude or phase spectra were observed under electrode rotation. Minor alterations were seen in some 2D electrode configurations, likely due to a higher level of anisotropy present on the tongue surface. The phase was again more stable than magnitude. Overall, the impedance phase appears stable during lateral measurements and electrode rotation.

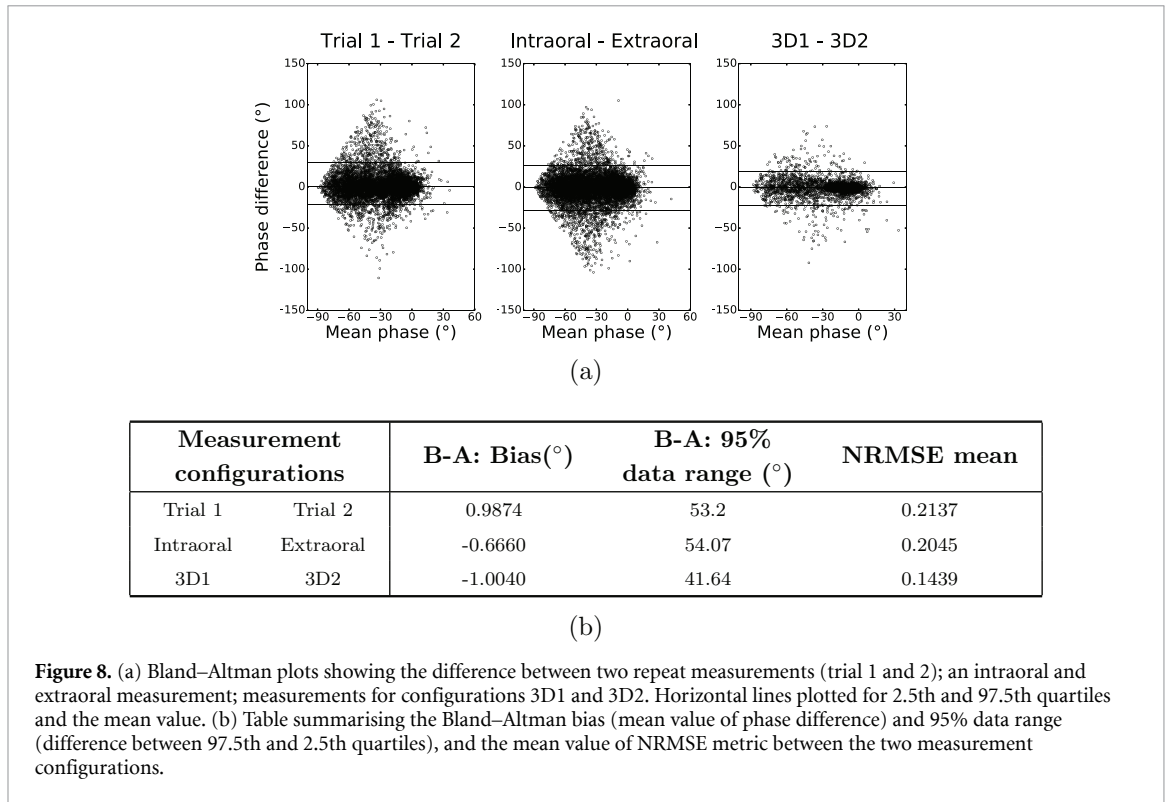


Figure 8. (a) Bland–Altman plots showing the difference between two repeat measurements (trial 1 and 2); an intraoral and extraoral measurement; measurements for configurations 3D1 and 3D2. Horizontal lines plotted for 2.5th and 97.5th quartiles and the mean value. (b) Table summarising the Bland–Altman bias (mean value of phase difference) and 95% data range (difference between 97.5th and 2.5th quartiles), and the mean value of NRMSE metric between the two measurement configurations.

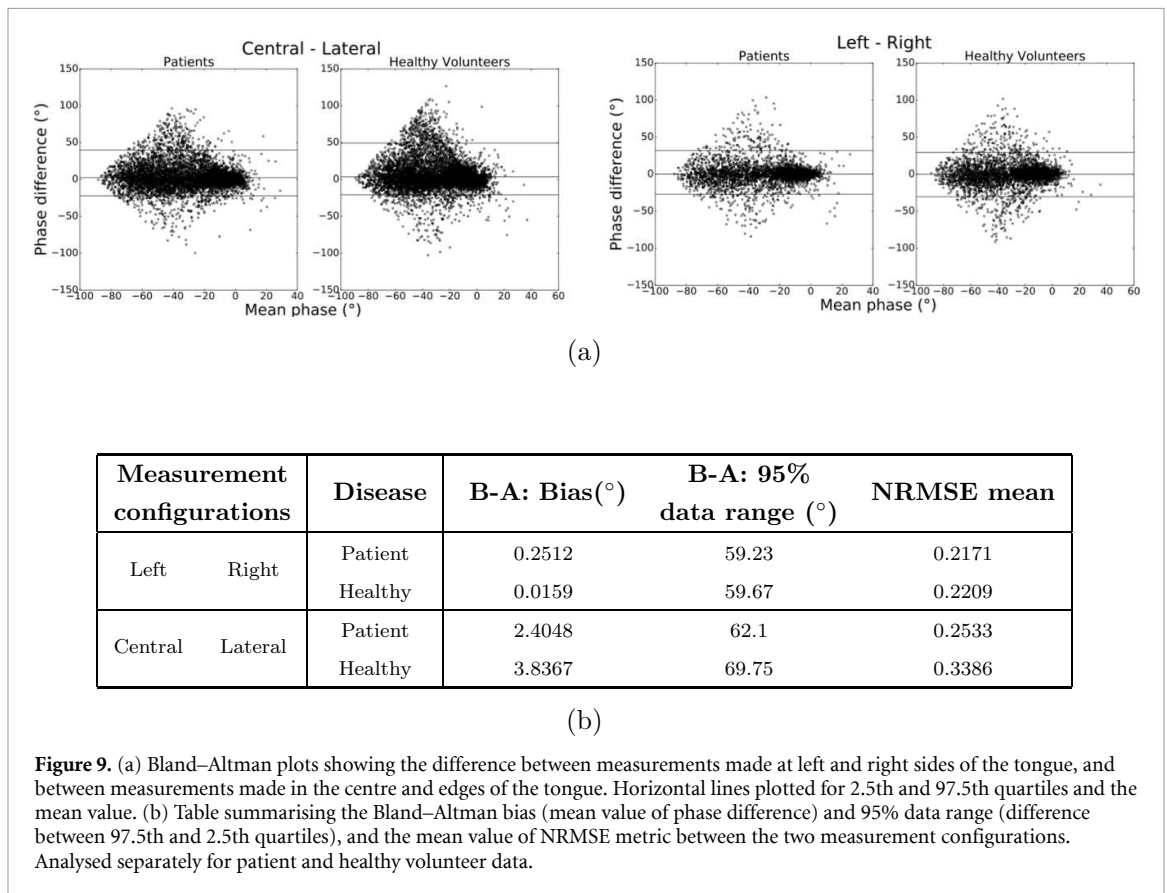


Figure 9. (a) Bland–Altman plots showing the difference between measurements made at left and right sides of the tongue, and between measurements made in the centre and edges of the tongue. Horizontal lines plotted for 2.5th and 97.5th quartiles and the mean value. (b) Table summarising the Bland–Altman bias (mean value of phase difference) and 95% data range (difference between 97.5th and 2.5th quartiles), and the mean value of NRMSE metric between the two measurement configurations. Analysed separately for patient and healthy volunteer data.

3.2.2. Variability of measurement configurations

All recordings were performed twice (trial 1 and trial 2) to allow for analysis of reproducibility. Some participants (both patients and healthy volunteers) found extraoral recordings difficult and thus all recording paradigms were not possible in every individual. Bland-Altman plots and the NRMSE (11) were used to assess spectral agreement/similarity between measurement configurations. The Bland–Altman mean

Table 2. Description of clinical examination scoring. An experienced physician (JJPA) gives a score in each of the three categories (wasting, weakness and fasciculations). The overall clinical score is then calculated as the sum of the three scores.

Clinical sign	Description and corresponding score			
Tongue wasting	None: 0	Minimal: 1	Moderate: 2	Severe: 3
Tongue weakness	None: 0	Movement inside and outside mouth: 1	Movement only inside mouth: 2	Paresis: 3
Fasciculations	Absent: 0	Present: 1		

Table 3. Reproducibility analysis. Intraclass correlation coefficient shown for central and lateral measurements with patient data, healthy volunteer data and all participants pooled. 95% confidence interval for the ICC is shown in brackets.

Analysis	Central ICC (95% confidence interval)	Lateral ICC (95% confidence interval)
Pooled	0.903 (0.898–0.908)	0.907 (0.902–0.911)
Patients	0.926 (0.920–0.931)	0.915 (0.909–0.920)
Healthy Volunteers	0.876 (0.866–0.885)	0.896 (0.889–0.903)

difference reveals bias, and, since the data is non-parametric, the 95% difference range was calculated using percentiles (Bland and Altman 1999). If the spectral similarity between two measurement configurations is within that of two repeat measurements, then the two different measurement configurations can be treated as equivalent data types.

Spectral similarity was assessed between intra- and extraoral measurements and different device placement positions (centre, left, right). Comparison was also made between the two electrode configurations 3D1 and 3D2, which are identical apart from a 5 mm lateral shift in the measurement area (see figure 1). NRMSE and Bland–Altman analyses demonstrated that both intraoral-extraoral and 3D1–3D2 comparison were within the threshold of two repeat measurements (figure 8). Thus, measurements are unaffected by tongue protrusion and there are no local variations in tissue structure.

Evaluation of left placement vs. right placement also revealed a high level of spectral similarity within the limits of two repeat measurements (figure 9). This was the case for both ALS patients (for all disease severities, appendix B5) and healthy volunteers. This indicates that no asymmetry in disease is observed. The comparison between lateral and central placements shows the largest difference; bias was relatively high, suggesting that central measurements output a higher phase than lateral measurements. Both the Bland–Altman range and the NRMSE exceed that of trial 1–trial 2 comparison.

3.2.3. Measurement reliability

A single-measure, two-way mixed effects intra-class correlation coefficient (ICC) analysis was undertaken to assess the reproducibility of measurements. The reliability of phase measurements was high for patients and healthy volunteers across both central and lateral measurements (table 3).

In addition, inter- and intra-rater analyses demonstrate high reliability across different observers; this was maintained across patient visits (appendix B1).

3.3. Classification performance and symptom correlation assessment

Feature selection was applied to the performance of both central and lateral (left and right combined) datasets independently for each electrode configuration. Left and right data are combined on the grounds of having similar spectra (see figure 9).

In our analyses we found that lateral measurements AUROC outperform those made on the centre of the tongue (figure 10(a)). We then combined the lateral and central measurement data and found that the combined dataset outperformed the lateral measurement only dataset (figure 10(b)). In addition, comparison of left vs. right lateral measurements revealed an identical performance ($\Xi = 0$). Inspection of the features (frequencies) selected by the wrapper algorithm revealed a preponderance of frequencies in top half of our frequency range (appendix B6). Comparing the performance of the different electrode configurations resulted in a general improvement for the 3D configurations over the 2D, as was previously demonstrated in Alix *et al* (2020).

The correlation of impedance phase with tongue strength was also compared between the lateral, central and combined datasets. Figure 11 shows the correlation between EIM (selected features presented in

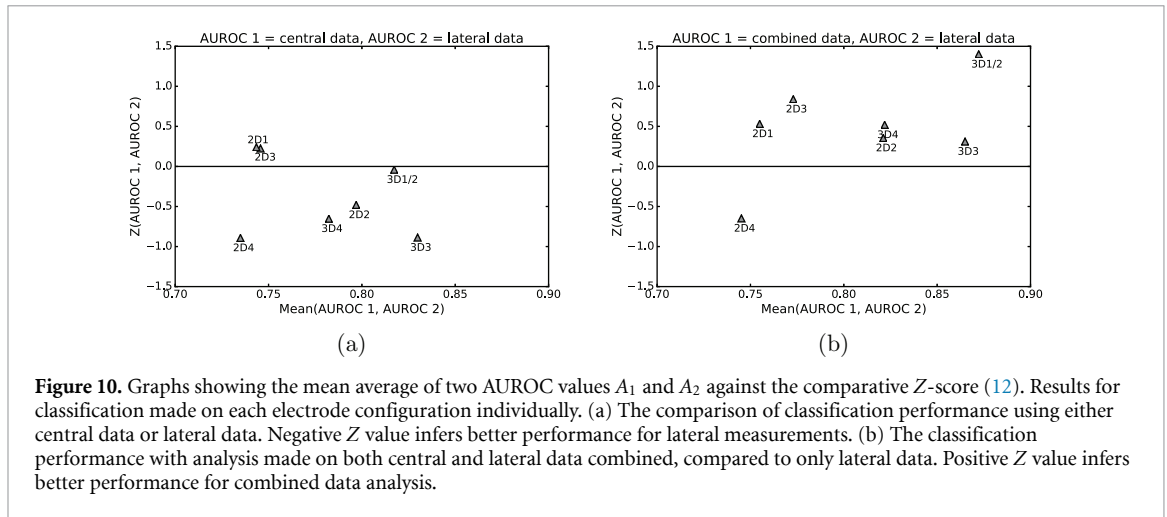


Figure 10. Graphs showing the mean average of two AUROC values A_1 and A_2 against the comparative Z-score (12). Results for classification made on each electrode configuration individually. (a) The comparison of classification performance using either central data or lateral data. Negative Z value infers better performance for lateral measurements. (b) The classification performance with analysis made on both central and lateral data combined, compared to only lateral data. Positive Z value infers better performance for combined data analysis.

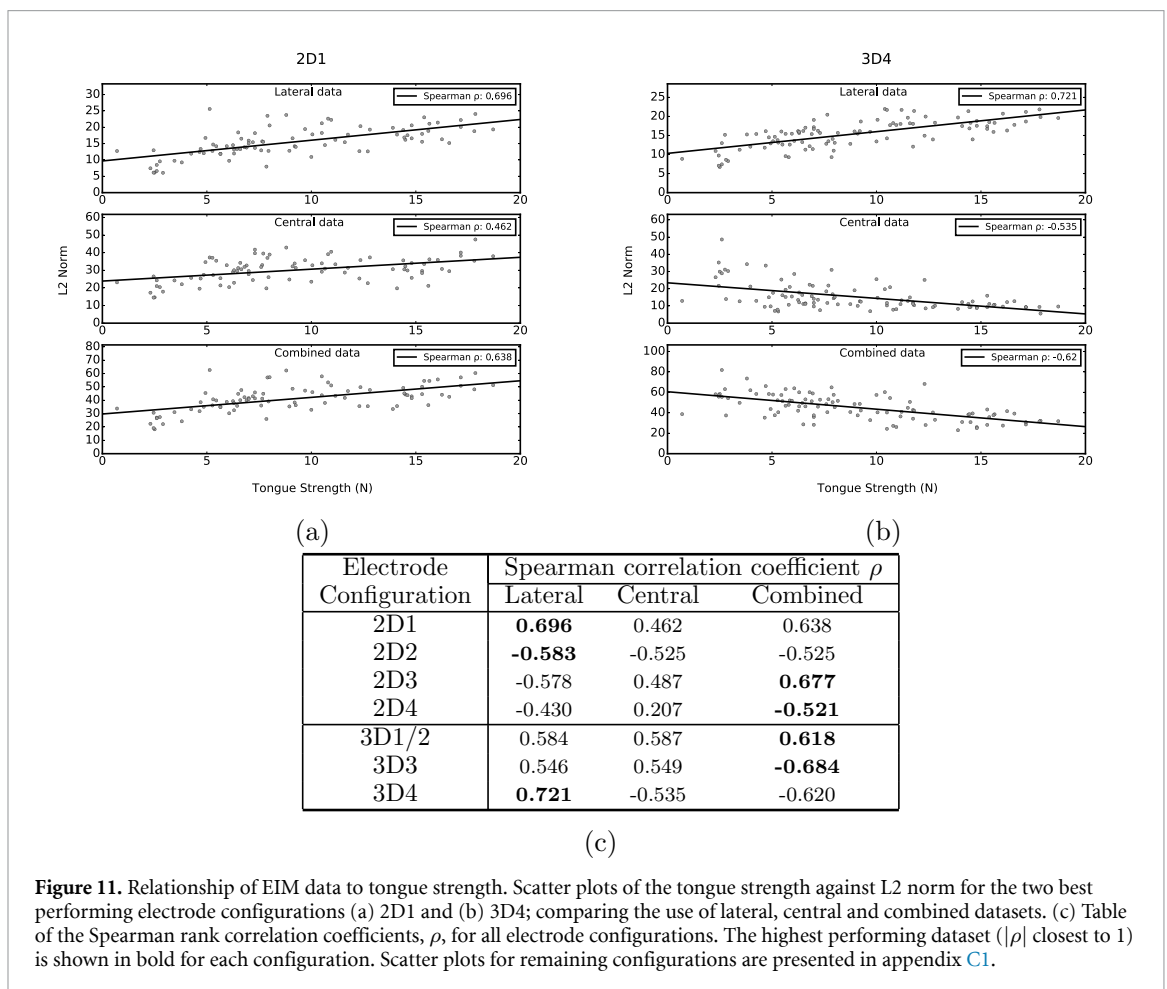


Figure 11. Relationship of EIM data to tongue strength. Scatter plots of the tongue strength against L2 norm for the two best performing electrode configurations (a) 2D1 and (b) 3D4; comparing the use of lateral, central and combined datasets. (c) Table of the Spearman rank correlation coefficients, ρ , for all electrode configurations. The highest performing dataset ($|\rho|$ closest to 1) is shown in bold for each configuration. Scatter plots for remaining configurations are presented in appendix C1.

appendix B7) and tongue strength for the highest performing 2D and 3D configurations (2D1 and 3D4), where best correlation was observed for the lateral datasets.

Comparing correlation coefficients between central, lateral and combined data for all configurations (figure 11(c)) shows consistent lowest performance for using central data. Both combined and lateral datasets perform well, with the overall best correlation observed for the lateral 3D4 dataset (Spearman $\rho = 0.72$).

4. Discussion

Previous FEM-based models of EIM have used impedance measurements of murine gastrocnemius muscle to obtain values for permittivity and conductivity (Pacheck *et al* 2016, Jafarpoor *et al* 2013, Jafarpoor *et al* 2011). This has the advantage of obtaining and using information taken directly from muscle preparations

but has the disadvantage of inputting results from muscle fibres of a different size to those in human subjects. Here, we have used a large dataset of over 9000 spectra from eight electrode configurations to develop a 3-dimensional model fitted to different stages of disease. Despite the difference in approach, our results align well with previous studies. For example, the small difference we observed on the effect of recording on the muscle edge concur with the conclusions of Pacheck *et al* whose FEM modelling on tongue EIM indicated that there is limited flow of current away from the electrodes (Pacheck *et al* 2016). Thus, while we did not utilise different tongue geometries for our patient and volunteer models, both our results and those of Pacheck *et al* suggest that changes in tongue volume are unlikely to impact upon measured or modelled spectra.

Edge effects have been reported in impedance imaging (Scholz and Anderson 2000, Li *et al* 2019). The minimal change to spectra observed in our studies may be explained by the variations seen in the impedance magnitude of the simulations. These observations imply that resistance and reactance are equally affected by any edge effects and therefore become insensitive to changes in phase but not magnitude. Phase angle is generally employed as the measured impedance parameter, since it is also deemed more resilient to changes in tissue size and effects of subcutaneous fat (Rutkove 2009, Rutkove *et al* 2007, Schwartz *et al* 2015, Li *et al* 2016). The slightly greater removal of outliers lateral data suggests that these recordings can still be subject to measurement error when electrodes loose contact with the tongue surface.

One limitation to our work is the use of central measurement data to optimise the FEM. However, the differences in central and lateral measurement spectra are small (figure 9) and much less prominent than the differences seen between the different patient groups. A future work could include generating models based on differing electrode placements in order to develop a more sophisticated 3D model.

Nonetheless, the application of our FEM to Cole-Cole circuit simulation results in changes to model parameters that are in keeping with the known pathophysiology of ALS. There are associated problems in attributing particular tissue properties directly to elements within the LT-Spice lumped parameter model, where the accuracy can be significantly affected by the approximations made (McAdams and Jossinet 1996). However, the capacitive element is differential to tissue permittivity and hence to cell membrane area within the tissue volume. Disease progression is associated with a loss of cell membranes and hence a reduction in the model capacitance is consistent with muscle cell atrophy. Increased extracellular resistance was also found and is in keeping with increases in extracellular connective tissue and fat known to occur in ALS (Rutkove 2009).

Our results also provide insight into the pathophysiology of tongue disease in ALS as the asymmetry typically observed in limb muscles was not seen in the tongue. This was the case across all severities of disease, suggesting that there is no asymmetry early on which is lost as the disease progresses. In keeping with the present results, it is our experience that clinically observable asymmetry of the tongue is not a feature of ALS. Cerebral hemispheric dominance has been suggested to be a driver of limb asymmetry (Henderson *et al* 2019); interestingly, the hypoglossal nucleus receives bilateral cortical innervation which may limit any such effect in the tongue muscle (Urban *et al* 1998, Chen *et al* 1999). There do, however, appear to be differences in the impedance spectra obtained from the centre of the tongue versus the lateral portions. Histological studies show a central band of connective tissue, the lingual septum (Larsson *et al* 1982), which may underlie such differences. It seems unlikely that the lingual septum will undergo any significant changes during ALS and thus central tongue EIM measurements will still be dominated by muscle. In keeping with this, both our group and others have shown that central placement is sensitive to disease and correlates with ALS symptoms (Alix *et al* 2020, Shellikeri *et al* 2015, McIllduff *et al* 2017).

During the collection of human data, we investigated intra- and extraoral recordings and found them to be similar. This is not surprising since extraoral protrusion is achieved via contraction of the genioglossus, and not the tongue blade from which recordings are made. Since some participants, mostly patients but some healthy volunteers, appeared to find extraoral recordings more difficult, this similarity indicates that the examiner can use whichever method is most comfortable for the participant.

As noted in our previous work, 3D electrode configurations appear to provide a superior performance to 2D arrangements. The reason for this remains undetermined but perhaps relates to the 3D configurations assessing a relatively greater amount of tongue muscle. Regardless of cause, this observation was preserved in both central and lateral placements. With regard to placement, classification performance across lateral and central measurements was high and correlation with tongue strength is observed in both datasets, suggesting pathology is occurring and detectable throughout the tongue. In general, however, lateral placement outperformed central placement. The underlying cause of the higher classification and tongue strength correlation from lateral measurements is unclear, although a purer assessment of muscle in lateral recordings (vs. muscle and the lingual septum in central recordings) may be a contributing factor. Nonetheless, classification appears enhanced through the incorporation of both lateral and central measurements and could be further assessed in a larger study.

5. Conclusion

In this paper we have further developed the technique of tongue EIM through a combination of FEM and detailed patient assessments. Our results show that lateral tongue measurements are technically and practically achievable. The data from lateral placement reveals symmetry in ALS tongue disease and, importantly, enhance disease identification. These data support the use of combined lateral and central tongue EIM measurements as a biomarker for ALS.

Acknowledgments

The work was funded by Ryder Briggs Trust/Neurocare, United Kingdom of Great Britain and Northern Ireland (Grant No. RS8470), the Motor Neurone Disease Association, United Kingdom of Great Britain and Northern Ireland (Grant No. 918-793) and an Engineering and Physical Sciences Research Council Doctoral Scholarship (Grant No. EP/R513313/1). The work was also supported by the NIHR Sheffield Biomedical Research Centre (BRC). PJS is supported as an NIHR Senior Investigator. The views expressed are those of the author(s) and not necessarily those of the NHS, the NIHR or the Department of Health.

The authors wish to thank the participants for their time and dedication. The author's have confirmed that any identifiable participants in this study have given their consent for publication.

Appendix A. Outlier removal algorithm

- (a) If any measurement set has resistance < 0 at any frequency the measurement set is removed.
- (b) **Repeat the following for impedance phase and impedance magnitude:**
For each configuration (c) and frequency (j) calculate the 'severe patient' median and quartiles (using only the data from patients presenting with severe symptoms, see appendix B1): $Q1_p^{cj}$, $Q2_p^{cj}$, $Q3_p^{cj}$.
For each set of measurements i in configuration c ($Z_c^i(f_j)$) calculate the RMSD (J_c^i) as:

$$J_c^i = \sqrt{\frac{1}{14} \sum_{j=1}^{14} \left(\frac{Z_c^i(f_j) - Q2_p^{cj}}{Q3_p^{cj} - Q1_p^{cj}} \right)^2}$$

For the variable J_c^i calculate the lower quartile, upper quartile and MedCouple: $Q1[J_c^i]$, $Q3[J_c^i]$, $MC[J_c^i]$. Define a threshold for each configuration:

$$T_c = Q3[J_c^i] + 3 * (Q3[J_c^i] - Q1[J_c^i]) * e^{4*MC[J_c^i]}$$

Then if: $J_c^i \geq T_c$ the full set of measurements i in configuration c is removed.

- (c) If any measurement set has phase $> 30^\circ$ at frequencies f_1 or f_{14} the measurement set is removed.

Appendix B. Tables

Table B1. Reproducibility analysis for final visit and inter-rater comparisons.

Analysis	ICC (95% confidence interval)	
	Central	Lateral
Patients	0.913	0.873
final visit	(0.903–0.922)	(0.861–0.885)
Intra-rater	0.903	0.907
	(0.898–0.908)	(0.902–0.911)
Inter-rater	0.870	0.866
	(0.859–0.880)	(0.858–0.875)

Table B2. Model parameters for the conductivity spectra in x , y and z directions and thickness of the upper, middle and lower sections of the tongue. For model of severe disease, moderate disease and healthy tissue.

section	Direction	Severe disease				Moderate disease				Healthy			
		Z_0	Z_1	F_C (Hz)	Thickness (mm)	Z_0	Z_1	F_C (Hz)	Thickness (mm)	Z_0	Z_1	F_C (Hz)	Thickness (mm)
Upper	x	15.1	4	530	2.31	26.4	4.4	260	2.17	20.5	2.9	380	2.03
	y	16.8	4.2	590		28.1	4.6	290		26.8	3.3	395	
	z	6.2	4.8	1.7×10^{-5}		7.1	4.5	1.4×10^{-5}		7.5	4.3	1.1×10^{-5}	
Middle	x	110	0.2	110	2.38	6.5	0.8	55	2.66	29	0.1	65	2.94
	y	45	0.1	280		29	0.1	65		7.2	0.1	60	
	z	210	0.2	200		235	1.5	60		180	0.1	35	
Lower	x	12.1	0.77	250	2.31	6.4	1.1	20	2.17	4.6	0.95	15	2.03
	y	10.6	0.75	250		17.5	1.2	25		5.8	1.15	15	
	z	12	9.6	1.7×10^{-5}		6.1	3.5	1.4×10^{-5}		9.2	4.4	1.1×10^{-5}	

Table B3. Normalised root mean square error (NRMSE) between central impedance spectra and spectra for shift A, B, C, D (see figure 5(a)). Shown for all electrode configurations for impedance magnitude and phase. NRMSE > 0.1 is shown in bold.

Shift	Severe disease				Moderate disease				Healthy			
	A	B	C	D	A	B	C	D	A	B	C	D
Magnitude NRMSE												
2D1	1.272	0.310	0.183	0.139	1.113	0.301	0.178	0.105	1.25	0.304	0.186	0.119
2D2	0.325	0.057	0.112	0.085	0.394	0.061	0.082	0.074	0.714	0.100	0.104	0.078
2D3	0.398	0.307	0.182	0.122	1.404	0.714	0.395	0.265	1.279	0.640	0.302	0.195
2D4	0.574	0.016	0.065	0.067	0.612	0.070	0.079	0.055	2.81	0.191	0.208	0.142
3D1	0.638	0.360	0.295	0.218	0.559	0.298	0.229	0.169	0.949	0.343	0.273	0.195
3D2	0.160	0.076	0.055	0.038	0.122	0.062	0.046	0.031	0.125	0.070	0.041	0.033
3D3	0.405	0.291	0.183	0.129	0.361	0.203	0.126	0.087	0.365	0.223	0.133	0.097
3D4	0.425	0.304	0.191	0.135	0.356	0.294	0.185	0.120	0.424	0.300	0.191	0.130
Phase NRMSE												
2D1	0.067	0.032	0.039	0.034	0.051	0.026	0.024	0.020	0.082	0.022	0.033	0.027
2D2	0.298	0.049	0.027	0.023	0.334	0.045	0.025	0.019	0.338	0.027	0.029	0.028
2D3	0.033	0.032	0.030	0.020	0.066	0.021	0.030	0.029	0.072	0.054	0.078	0.064
2D4	0.316	0.021	0.015	0.013	0.380	0.032	0.023	0.014	0.502	0.060	0.037	0.026
3D1	0.234	0.050	0.045	0.032	0.297	0.039	0.035	0.032	0.043	0.031	0.030	0.022
3D2	0.032	0.015	0.017	0.016	0.042	0.021	0.012	0.011	0.055	0.024	0.025	0.022
3D3	0.032	0.015	0.017	0.016	0.042	0.021	0.012	0.011	0.055	0.024	0.025	0.022
3D4	0.046	0.039	0.033	0.024	0.068	0.036	0.037	0.029	0.085	0.036	0.050	0.039

Table B4. Normalised root mean square error (NRMSE) between central impedance spectra and spectra for rotations of 45°, 30° and 15°. Shown for all electrode configurations for impedance magnitude and phase. NRMSE > 0.1 is shown in bold.

	Severe disease			Moderate disease			Healthy		
	Magnitude NRMSE								
Rotation	45°	30°	15°	45°	30°	15°	45°	30°	15°
2D1	0.020	0.012	0.011	0.041	0.040	0.006	0.097	0.058	0.035
2D2	0.023	0.010	0.002	0.022	0.014	0.007	0.054	0.029	0.021
2D3	0.041	0.028	0.007	0.468	0.160	0.021	0.188	0.098	0.040
2D4	0.043	0.028	0.010	0.188	0.109	0.031	0.183	0.127	0.051
3D1	0.003	0.004	0.001	0.021	0.010	0.002	0.027	0.021	0.014
3D2	0.003	0.003	0.003	0.008	0.004	0.003	0.026	0.016	0.002
3D3	0.005	0.007	0.001	0.008	0.004	0.003	0.020	0.004	0.012
3D4	0.005	0.004	0.001	0.012	0.004	0.006	0.025	0.007	0.006
	Phase NRMSE								
2D1	0.045	0.031	0.005	0.064	0.044	0.018	0.100	0.083	0.039
2D2	0.026	0.015	0.004	0.021	0.011	0.006	0.043	0.024	0.012
2D3	0.026	0.015	0.008	0.240	0.098	0.018	0.037	0.015	0.006
2D4	0.021	0.010	0.008	0.209	0.102	0.028	0.049	0.031	0.012
3D1	0.008	0.011	0.003	0.015	0.009	0.008	0.024	0.015	0.010
3D2	0.007	0.006	0.003	0.017	0.011	0.007	0.018	0.011	0.005
3D3	0.007	0.005	0.002	0.022	0.012	0.003	0.017	0.009	0.006
3D4	0.007	0.004	0.002	0.025	0.013	0.006	0.016	0.007	0.004

Table B5. Asymmetry analysis at different symptom severities. The difference between left and right measurements is quantified through Bland–Altman (B-A) analysis (columns 1 and 2) and the NRMSE metric (column 3). Variation in the left and right spectra neither increases nor decreases with disease.

Symptoms	B-A: Bias(°)	B-A: data range (°)	NRMSE mean
None	1.1187	55.21	0.2195
Mild	−0.3454	63.28	0.2866
Moderate	0.7829	51.95	0.1842
Severe	0.8679	54.00	0.2494

Table B6. Classification performance comparison between (a) lateral data, (b) central data, and (c) both data types combined. For each electrode configuration 3-nearest neighbour, 4-fold cross validation with forward selection wrapper method algorithm applied to select a maximum of eight features.

Lateral data classification				
	Features	AUROC	Sensitivity	Specificity
2D1	f9, f12, f13	0.74	0.69	0.79
2D2	f10, f12	0.81	0.84	0.79
2D3	f1, f11	0.73	0.71	0.76
2D4	f3, f6, f11, f12, f13, f14	0.77	0.75	0.79
3D1/2	f9, f10, f12, f14	0.82	0.71	0.92
3D3	f3, f5, f9, f10, f11, f12, f13, f14	0.86	0.90	0.81
3D4	f8, f11, f13, f14	0.81	0.81	0.8
Central data classification				
	Features	AUROC	Sensitivity	Specificity
2D1	f11, f12	0.75	0.79	0.71
2D2	f9, f12, f13	0.78	0.74	0.82
2D3	f5, f6, f7, f8, f9, f12, f13, f14	0.75	0.59	0.92
2D4	f1, f12, f14	0.70	0.5	0.90
3D1/2	f2, f5, f9, f10, f11, f12	0.82	0.79	0.85
3D3	f10, f11, f13	0.80	0.79	0.81
3D4	f6, f12, f13	0.76	0.75	0.77
Combined data classification				
	Features	AUROC	Sensitivity	Specificity
2D1	Central: f8 Lateral: f11, f12	0.77	0.76	0.79
2D2	Central: f8 Lateral: f10	0.83	0.84	0.82
2D3	Central: f4, f9 Lateral: f1, f9	0.79	0.71	0.88
2D4	Central: f1, f3 Lateral: f12, f14	0.72	0.44	1.0
3D1/2	Central: f1, f11, f13 Lateral: f9, f13	0.91	0.89	0.92
3D3	Central: f11, f13 Lateral: f12	0.87	0.90	0.85
3D4	Central: f9, f11, f12, f13 Lateral: f14	0.84	0.88	0.8

Table B7. Features selected through forward selection wrapper for L2 norm phase impedance correlation with tongue strength.

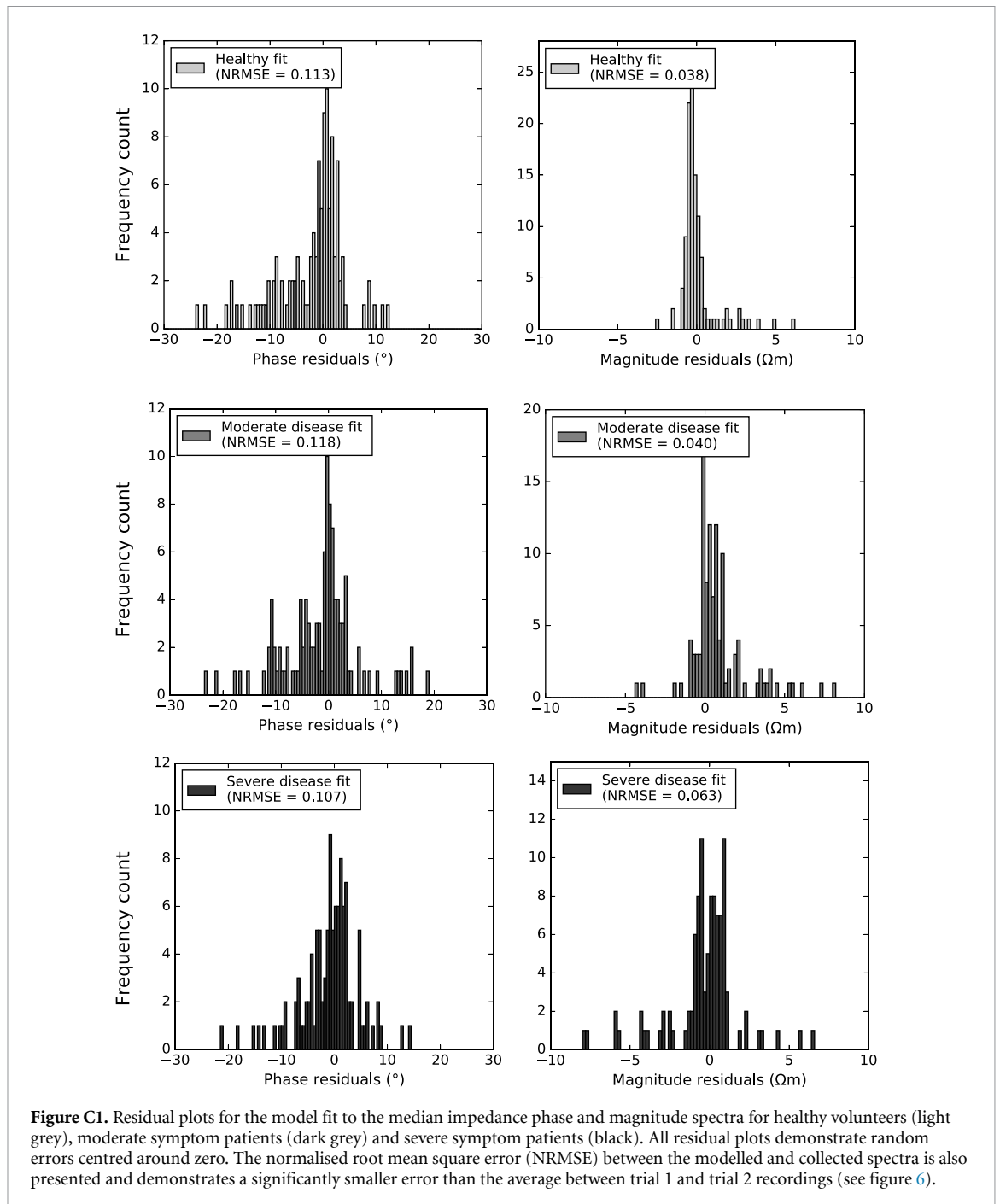
Lateral data		Central data	
	Features		Features
2D1	f1, f12	2D1	f1, f2, f9, f10, f12, f13, f14
2D2	f6, f14	2D2	f5, f13
2D3	f3, f5	2D3	f11
2D4	f4	2D4	f1, f8, f10, f13, f14
3D1/2	f3, f10, f11, f12, f14	3D1/2	f1, f12
3D3	f1, f2, f11, f13, f14	3D3	f11
3D4	f13	3D4	f6, f14

(a) (b)

Combined data		
	Features	
	Lateral	Central
2D1	f1, f2, f3, f11, f12, f13, f14	f9, f10, f11, f12, f13, f14
2D2	-	f5, f13
2D3	f13	f12
2D4	f4	f5
3D1/2	f1, f10, f12	f1, f2, f12
3D3	f6	f4
3D4	f5, f9	f1, f5, f6, f7, f9, f10, f14

(c)

Appendix C. Figures



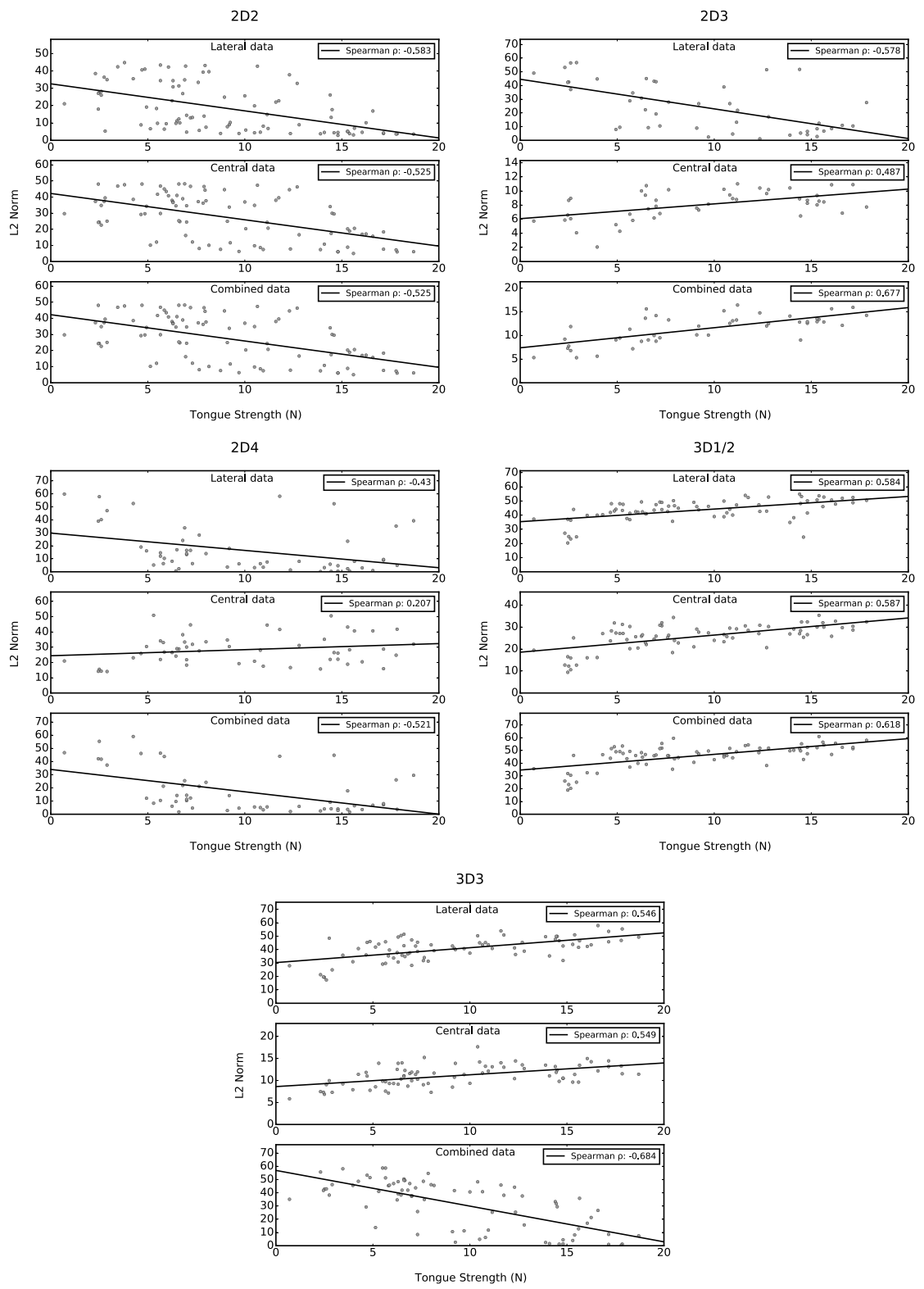


Figure C2. Scatter plots of the tongue strength against L2 norm for the remaining electrode configurations not presented in section 3.3.

References

- Alix J J P, McDonough H E, Sonbas B, French S J, Rao D G, Kadirkamanathan V, McDermott C J, Healey T J and Shaw P J 2020 Multi-dimensional electrical impedance myography of the tongue as a potential biomarker for amyotrophic lateral sclerosis *Clin. Neurophysiol.* **131** 799–808
- Anumba D O, Stern V, Healey T J, Dixon S and Brown B H 2020 The value of cervical electrical impedance spectroscopy to predict spontaneous preterm delivery in asymptomatic women: the ECCLIPx prospective cohort study *Ultrasound Obstet. Gynecol.* accepted (<https://doi.org/10.1002/uog.22180>)
- Benatar M, Boylan K, Jeromin A, Rutkove S B, Berry J, Atassi N and Brujin L 2016 ALS biomarkers for therapy development: state of the field and future directions *Muscle Nerve* **53** 169–82
- Bishop C 2006 *Pattern Recognition and Machine Learning* (Berlin: Springer)
- Bland J M and Altman D G 1999 Measuring agreement in method comparison studies *Stat. Methods Med. Res.* **8** 135–60
- Chen C H, Wu T S and Chu N 1999 Bilateral cortical representation of the intrinsic lingual muscles *Neurology* **52** 411–13
- Devine M, Kiernan M, Pannek K, Stephen R, McCombe P and Henderson R 2014 28. Asymmetry of motor dysfunction in amyotrophic lateral sclerosis: the effect of limb dominance *Clin. Neurosci.* **21** 2042
- Easterling C, Antinola J, Cashin S and Barkhaus P E 2013 Changes in tongue pressure, pulmonary function and salivary flow in patients with amyotrophic lateral sclerosis *Dysphagia* **28** 217–25
- Gaige T A, Benner T, Wang R, Wedeen V J and Gilbert R J 2007 Three dimensional myoarchitecture of the human tongue determined in vivo by diffusion tensor imaging with tractography *J. Magn. Reson. Imaging* **26** 654–61
- Gilbert R J and Napadow V J 2005 Three-dimensional muscular architecture of the human tongue determined in vivo with diffusion tensor magnetic resonance imaging *Dysphagia* **20** 1–7
- Hanley J A and Hajian-Tilaki K O 1997 Sampling variability of nonparametric estimates of the areas under receiver operating characteristic curves: an update *Acad. Radiol.* **4** 49–58
- Henderson R D, Garton F D, Kiernan M C, Turner M R and Eisen A 2019 Human cerebral evolution and the clinical syndrome of amyotrophic lateral sclerosis *J. Neurol. Neurosurg. Psychiatry* **90** 570–75
- Hopkin G B 1967 Neonatal and adult tongue dimensions *Angle Orthod.* **37** 132–33
- Hua P, Woo E J, Webster J G and Tompkins W J 1993 Finite element modeling of electrode–skin contact impedance in electrical impedance tomography *IEEE Trans. Biomed. Eng.* **40** 335–43
- Jafarpour M, Li J, White J K and Rutkove S B 2013 Optimizing electrode configuration for electrical impedance measurements of muscle via the finite element method *IEEE Trans. Biomed. Eng.* **60** 1446–452
- Jafarpour M, Spieker A, Li J, Sung M, Darras B T and Rutkove S B 2011 Assessing electrical impedance alterations in spinal muscular atrophy via the finite element method *2011 Annual Int. Conf. IEEE Engineering in Medicine and Biology Society* pp 1871–874
- Khan S, Mahara, A, Hyams E S, Schned A R and Halter R J 2016 Prostate cancer detection using composite impedance metric *IEEE Trans. Med. Imaging* **35** 2513–523
- Lackovic I and Stare Z 2007 Low-frequency dielectric properties of the oral mucosa *13th Int. Conf. Electrical Bioimpedance and the 8th Conf. Electrical Impedance Tomography* vol 17
- Larsson S G, Mancuso A and Hanafee W 1982 Computed tomography of the tongue and floor of the mouth *Radiology* **143** 493–500
- Li J, Ji Z, Liu B, Shi X and Dong X 2019 Influence of the measuring probe structure on the electrical-field edge effect in electrical impedance scanning *Med. Imaging Health Inform.* **1** 47–52
- Li L, Li X, Hu H, Shin H and Zhou P 2016 The effect of subcutaneous fat on electrical impedance myography: electrode configuration and multi-frequency analyses *PLoS One* **11** 5
- McAdams E T and Jossinet J 1996 Problems in equivalent circuit modelling of the electrical properties of biological tissues *Bioelectrochem. Bioenerg.* **40** 147–52
- McIllduff C E, Yim S J, Pacheck A K and Rutkove S B 2017 Optimizing electrical impedance myography of the tongue in amyotrophic lateral sclerosis *Muscle Nerve* **55** 539–43
- Ong C K and Chong V F 2006 Imaging of tongue carcinoma *Cancer Imaging* **6** 186–93
- Pacheck A, Mijailovic A, Yim S, Li J, Green J R, McIllduff C E and Rutkove S B 2016 Tongue electrical impedance in amyotrophic lateral sclerosis modeled using the finite element method *Clin. Neurophysiol.* **127** 1886–890
- Prestin S, Rothschild S I, Betz C S and Kraft M 2012 Measurement of epithelial thickness within the oral cavity using optical coherence tomography *Head Neck* **34** 1777–781
- Richter I, Alajbeg I, Vučićević Boras V, Andabak Rogulj A and Brailo V 2015 Mapping electrical impedance spectra of the healthy oral mucosa: a pilot study *Acta Stomatol. Croat.* **49** 331–39
- Rutkove S B 2009 Electrical impedance myography: background, current state and future directions *Muscle Nerve* **40** 936–46
- Rutkove S B, Zhang H, Schoenfeld D A, Raynor E A, Shefner J M, Cudkowics M E, Chin A B, Aaron R and Shiffman C A 2007 Electrical impedance myography to assess outcome in amyotrophic lateral sclerosis clinical trials *Clin. Neurophysiol.* **118** 2413–418
- Sanchez B, Pacheck A and Rutkove S B 2016 Guidelines to electrode positioning for human and animal electrical impedance myography research *Sci. Rep.* **6** 32615 (<https://www.nature.com/articles/srep32615>)
- Scholz B and Anderson R 2000 On electrical impedance scanning—principles and simulations *Electromedica* **68** 35–44
- Schwartz S, Geisbush T R, Mijailovic A, Pasternak A, Darras B T and Rutkove S B 2015 Optimizing electrical impedance myography measurements by using a multifrequency ratio: a study in Duchenne muscular dystrophy *Clin. Neurophysiol.* **126** 202–08
- Shefner J M, Rutkove S B, Caress J B, Benatar M, David W S, Cartwright M S, Macklin E A and Bohorquez J L 2018 Reducing sample size requirements for future ALS clinical trials with a dedicated electrical impedance myography system *Amyotrop. Lateral Scler. Frontotemporal Degener.* **19** 555–61
- Shellicker S, Yunusova Y, Green J R, Pattee G L, Berry J D, Rutkove S B and Zinman L 2015 Electrical impedance myography in the evaluation of the tongue musculature in amyotrophic lateral sclerosis *Muscle Nerve* **52** 584–91
- Shiffman C A and Rutkove S B 2013a Circuit modeling of the electrical impedance: I. neuromuscular disease *Physiol. Meas.* **34** 203–21
- Shiffman C A and Rutkove S B 2013b Circuit modeling of the electrical impedance: II. Normal subjects and system reproducibility *Physiol. Meas.* **34** 223–35
- Urban P P, Vogt T and Hopf H C 1998 Corticobulbar tract involvement in amyotrophic lateral sclerosis. a transcranial magnetic stimulation study *Brain* **121** 1099–108